Surface Review and Letters, Vol. 5, No. 6 (1998) 1249-1256

SMART: AN ABERRATION-CORRECTED XPEEM/LEEM WITH ENERGY FILTER

R. WICHTENDAHL,* R. FINK,†[a] H. KUHLENBECK,* D. PREIKSZAS,‡
H. ROSE,‡ R. SPEHR,‡ P. HARTEL,‡ W. ENGEL,* R. SCHLÖGL,*
H.-J. FREUND,* A. M. BRADSHAW,* G. LILIENKAMP,‖
TH. SCHMIDT,‖ E. BAUER,§‖ G. BENNER¶ and E. UMBACH†[b]

Fritz-Haber-Insitut der Max-Planck-Gesellschaft, Faradayweg 4-6, D-14195 Berlin, Germany

†Universität Würzburg, Experimentelle Physik II, Am Hubland, D-97074 Würzburg, Germany

‡Technische Hochschule Darmstadt, Angewandte Physik, Hochschulstr. 6, D-64289 Darmstadt, Germany

§Technische Universität Clausthal, Leibnizstr. 4, D-38678 Clausthal-Zellerfeld, Germany

‖Arizona State University, Department of Physics and Astronomy, Tempe, AZ85287-1504, USA

¶LEO Elektronenmikroskopie GmbH, D-73446 Oberkochen, Germany

Received 1 September 1998

A new UHV spectroscopic X-ray photoelectron emission and low energy electron microscope is presently under construction for the installation at the PM-6 soft X-ray undulator beamline at BESSY II. Using a combination of a sophisticated magnetic beam splitter and an electrostatic tetrode mirror, the spherical and chromatic aberrations of the objective lens are corrected and thus the lateral resolution and sensitivity of the instrument improved. In addition a corrected imaging energy filter (a so-called omega filter) allows high spectral resolution (ΔE = 0.1 eV) in the photoemission modes and background suppression in LEEM and small-spot LEED modes. The theoretical prediction for the lateral resolution is 5 Å; a realistic goal is about 2 nm. Thus, a variety of electron spectroscopies (XAS, XPS, UPS, XAES) and electron diffraction (LEED, LEEM) or reflection techniques (MEM) will be available with spatial resolution unreached so far.

1. Introduction

Combining various photoelectron spectroscopy techniques (UPS, XPS, XAES) and X-ray absorption with nanoscopic resolution is doubtless extremely important for many fields in surface science. Although scanning tunneling microscopy (STM) and related scanning probe techniques have revolutionized the field by directly imaging surfaces on an atomic scale, they are not appropriate tools for extracting spectroscopic information. This holds in particular for STM, since the conditions of the scanning tip drastically influence the tunneling conditions and thus the obtained "spectroscopic" information is sometimes doubtful.

In low energy electron microscopy (LEEM), structural information on the length scale of a few nanometers can be obtained.[1] Although the lateral resolution reached so far is worse than for STM, LEEM has developed into a valuable technique for

[a]Corresponding author. E-mail: raifi@physik.uni-wuerzburg.de
[b]Project coordinator.

studying, for example, *in situ* film growth. In combining a LEEM with an energy filter and electron excitation by monochromatic X-rays ("XPEEM"), such an instrument becomes even more powerful, since then the well-established photoemission and X-ray absorption techniques can directly be correlated with structural properties on a similar length scale. This has been demonstrated for the Clausthal LEEM when mounted to high brilliance undulators at BESSY-I[2] and ELETTRA.[3]

The limiting factor in spatial resolution in both XPEEM and LEEM is mainly the influence of axial aberrations. In order to circumvent these limitations, Rose and Preikszas proposed a device for correction of spherical and chromatic aberrations consisting of a magnetic beam splitter and an electrostatic tetrode mirror. Recently, Rempfer *et al.* have demonstrated experimentally that such a device can indeed be utilized as an aberration corrector.[4] Research groups of five German research institutions have decided to jointly develop a versatile and high performance spectromicroscope called SMART, which uses this aberration correction device.[5] In this instrument, an aberration correction of the objective lens in combination with an aberration corrected imaging energy filter then allows one to study geometric properties of surfaces as well as physical and chemical processes with a spatial resolution of well below 5 nm using many different spectroscopic techniques.

In this paper we will briefly describe the effect of aberration correction on the lateral resolution (Sec. 2) and the general layout of this instrument (Sec. 3), which has been published in more detail recently.[5] The versatility of the SMART spectromicroscope will be demonstrated by the numerous modes of operation (Sec. 4). In addition, some estimations will be given on the effect of the sample heat load using the high brilliance undulator source at BESSY-II.

2. Aberration Correction

As mentioned above, the crucial point in an electron microscope is the influence of aberrations of the objective lens. There are several ways to correct for aberrations, which have been investigated theoretically for example by Rose[6] and Zach.[7] To simultaneously correct for spherical and chromatic aberrations, there are three possibilities in principle: (1) a combination of electric–magnetic quadrupoles with an octupole to independently correct for chromatic and spherical aberrations, respectively;[7] (2) a Wien filter in between to hexapoles;[6] (3) an electron mirror.[8] In the electron mirror concept, the reversal of the electrons after deceleration to zero kinetic energy and subsequent acceleration within the mirror induce chromatic and spherical aberrations opposite to those of round lenses and thus cancel out in a highly symmetric setup.[9] The restrictions (such as stability requirements of the electric power supplies) that are necessary for realizing the first two concepts are very demanding, and therefore the third alternative is preferable.

Figure 1 compares the resolution limit and the acceptance angle of the objective lens with and without correction by an electrostatic tetrode mirror as it will be used in the SMART. The data (solid lines) are calculated for vanishing electric field strength (a mode that can be realized in SMART) at the sample for a kinetic energy of 500 eV, i.e. typical values for X-ray photoelectrons. The dashed line describes the acceptance angle in the object plane. The (theoretical) resolution limit improves from about 10 nm to 0.5 nm upon aberration correction (with simultaneously improved sensitivity). For equal resolution the correction yields significantly larger

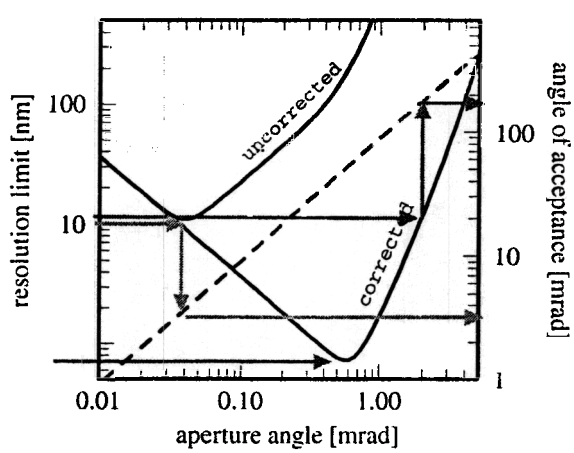

Fig. 1. Resolution limit and angle of acceptance in the case of a field-free object and an emission energy of 500 V: an energy window of 2 eV has been assumed for the energy filter. The solid lines represent the resolution limit as a function of the beam aperture at the entrance of the electron mirror for the corrected and the uncorrected case; the dashed line describes the angle of acceptance in the object plane.

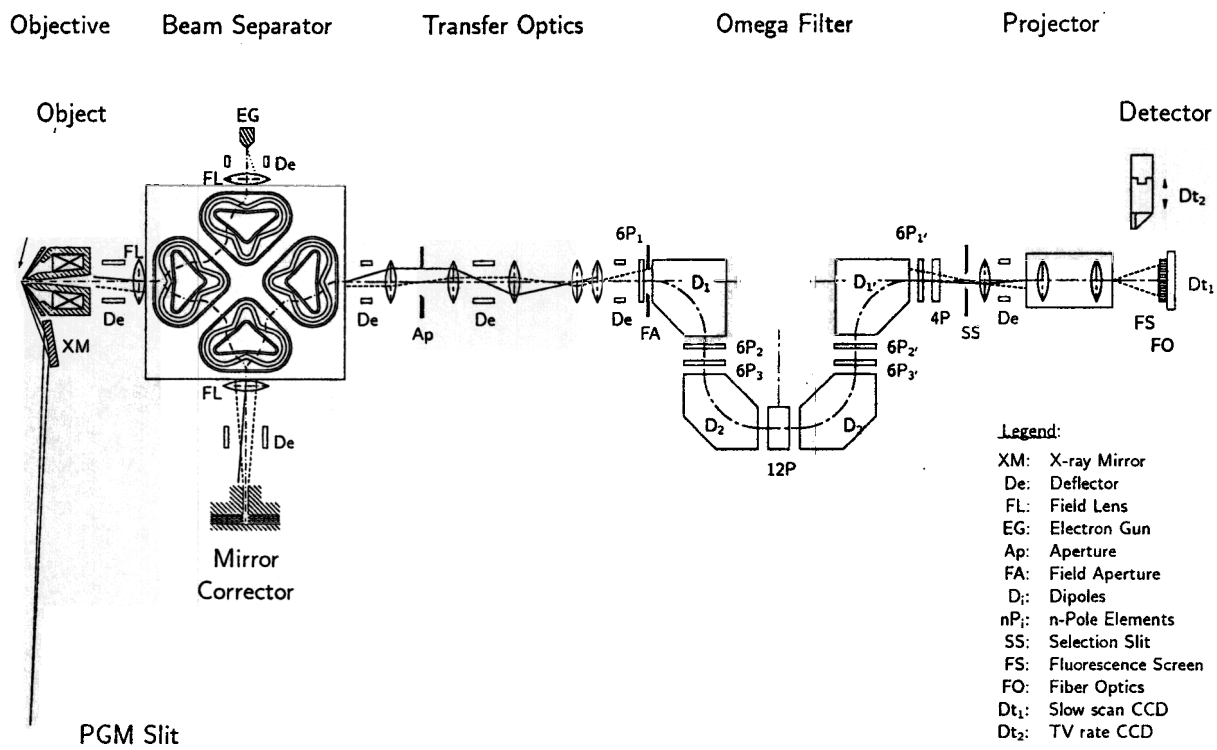

Fig. 2. Schematic layout of the new spectromicroscope SMART, presently under construction for BESSY II.

acceptance angles and thus a much higher transmission (about a factor 3000), as indicated in Fig. 1 by the horizontal and vertical arrows. This improvement of transmission is an important prerequisite for high lateral resolution, because the number of image-forming electrons is relatively small in the case of high energy photoelectrons, and the signal-to-noise ratio scales inversely with the square root of the total number of electrons.

3. The SMART Concept

The layout of the SMART spectromicroscope is schematically shown in Fig. 2. The sample which is illuminated by monochromatized X-rays at 20° glancing incidence is located in front of the objective lens. The magnetic beam splitter deflects the the photoemitted, diffracted or reflected electrons from the objective lens to the tetrode mirror and from there through a transfer lens system into the imaging energy filter without introducing further aberrations. Additionally, an electron beam from a field emission gun located opposite to the tetrode mirror can be coupled in to illuminate the sample through the objective lens. The omega filter is used as an energy-selecting device. The aberrations of this filter are corrected to second order and thus the spatial information is preserved. Finally, the energy-filtered image is projected onto an image intensifier which is directly coupled by fiber optics to a slow scan CCD camera. The whole instrument will be fully computer-controlled in order to perform the different modes of operation without time-consuming optimization procedures. The operation voltage of the electron imaging column (and the bias voltage of the sample) will be 15 kV.

3.1. *Objective lens and aberration corrector*

The objective lens is designed as an electrostatic–magnetic compound lens using the sample as cathode ("immersion lens"). The magnetic pole piece can be set to a negative potential which allows one to reduce the electrical field strength at the sample to zero. The lens forms an intermediate image at the entrance of the beam splitter, where a field lens sets the source position to infinity. The signs of the third order spherical and second rank chromatic aberrations of the tetrode mirror[10] are opposite to those of

the objective lens and thus cancel each other. The key component is the beam splitter,[8] which is corrected to second order due to symmetry and does not introduce dispersion. It consists of eight coil triplets residing in grooves of the pole pieces. A thin wall vacuum chamber made of OFHC-copper with a total thickness of 7 mm is mounted in between the pole pieces to let the electrons pass the complicated way through the beam splitter which is indicated by the dashed lines in Fig. 2.

3.2. *Transfer optics and Ω energy filter*

The five einzel lenses of the transfer optics project the source (diffraction pattern) and sample image onto the first and the second entrance plane of the omega-filter,[11] respectively, independent of the selected magnification. The images at the entrance planes (see Fig. 2) can be interchanged in order to obtain energy-filtered LEED patterns. The Ω filter consists of four sector magnets, each deflecting the electrons by 90°. All the geometric second rank aberrations are canceled out by symmetry and by the fields of the 6- and 12-pole elements. The dispersion is 35 μm/eV at 15 keV pass energy in the dispersion plane ("SS" in Fig. 2). A set of exchangeable high precision slits is used to choose the appropriate electron energy.

3.3. *Sample handling and manipulation*

One of the main obstacles in high resolution electron microscopy is mechanical stability. Therefore, the specimen chamber has been machined from one solid piece. The samples can be positioned within an x–y range of ±5 mm, with a reproducibility of 1 μm. The sample surface normal can be aligned precisely along the objective axis. Vibrations are damped by insulating frictional bearings mounted between sample holder and objective lens. Manipulators of this type have proven to be stable against vibrations and thermal effects within the nm range in the Clausthal LEEM.[12,13] Samples with 10–14 mm diameter may be mounted on a transferable sample holder. Electron bombardment heating and LN_2 cooling allow sample temperatures from 200 K to 2300 K.

3.4. *The photon source: PM-6 monochromator at BESSY II*

Since X-ray induced electron emission processes will mainly be used for imaging in the SMART instrument, high spectral resolution and brilliance is required. Therefore, a newly developed high resolution, high flux soft X-ray plane grating monochromator at a BESSY-II 49 mm period undulator named PM-6 will provide soft X-rays in

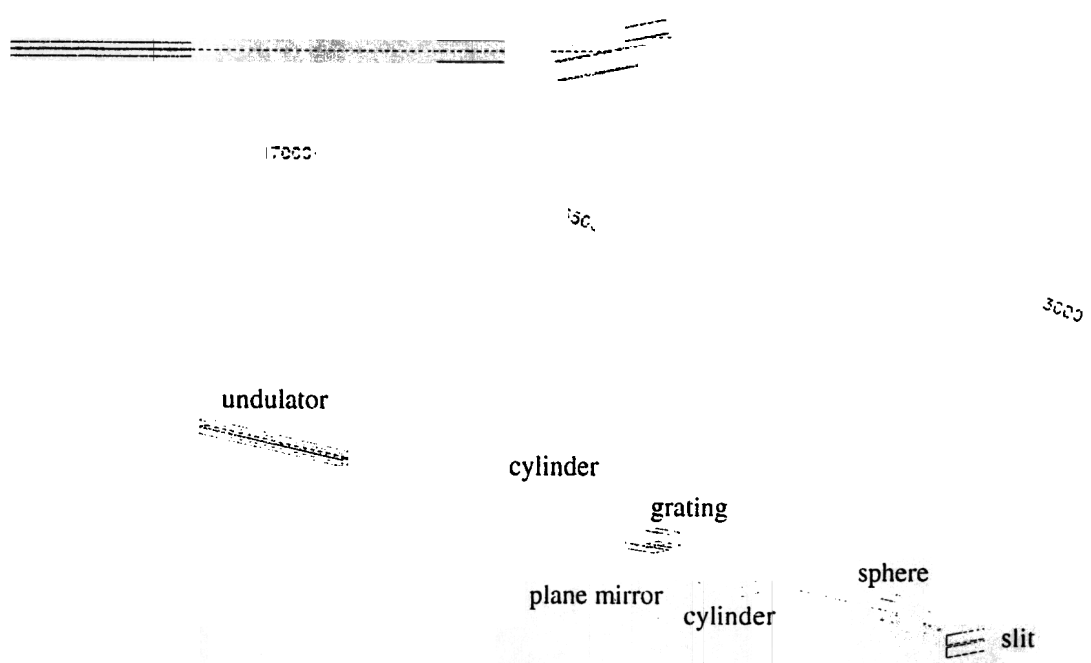

Fig. 3. Optical setup of the high flux, high resolution PM6 beamline at BESSY II.

the energy range of about 100 to 2000 eV.[14] The monochromator may be regarded as a further refinement of the Petersens SX700 concept.[15] The grazing incidence plane grating and its corresponding plane mirror are the only vertically (the dispersion direction) deflecting elements. Therefore, the slope errors of these plane elements mostly affect the resolving power. The optical setup is shown in Fig. 3. Due to collimation of the beam by the first mirror, it is possible to position the two foci of the demagnified source independently in the fixed exit slit. Refocusing by a toroidal mirror (later by a set of elliptical mirrors) demagnifies the beam onto a 10×25 μm^2 spot on the sample. For an exit slit width of 10 μm the resolving power of the PM-6 using the 1200 lines/mm grating is calculated to be 14.000 at a photon energy of 400 eV. The photon flux density is estimated to be 10^{10} s^{-1} μm^{-2}. The use of an interchangeable grating with 360 lines/mm increases the photon flux by about a factor of 10 at the expense of energy resolution. The spectromicroscope will be installed about 2.5 m from the monochromator exit slit behind a high resolution photoemission and X-ray fluorescence setup. Switching between these two experimental stations will be possible within minutes.

3.5. *Sample preparation*

The measurement chamber has several ports to facilitate *in situ* controlled gas exposure and evaporation. For purposes going beyond this, a separate UHV chamber is mounted vibrationally decoupled next to the microscope. It allows quick sample introduction and storage, sputtering, gas exposure, LEED/Auger and gas analysis with a quadrupole mass spectrometer. Metal evaporation sources and devices for organic and semiconductor film preparation can also be attached.

4. Modes of Operation

The combination of synchrotron radiation with a low energy emission microscope equipped with an energy filter provides great versatility for spectroscopic imaging of surfaces. In particular, the following modes of operation will be available in the SMART instrument.

4.1. *Photoelectron microscopy*

The monochromator provides photons to excite valence and core electrons. A broad variety of well-established spectroscopies will be available with unsurpassed spatial resolution.

4. 1 *Fixed $h\nu$ and E_{kin} (X)PEEM*

- 0 eV $< E_{kin} <$ 5 eV: The work function and its local changes are imaged. The electrons are usually excited using a conventional Hg high pressure lamp as UV source.
- 30 eV $< E_{kin} <$ 100 eV: Optimal surface sensitivity is achieved.
- E_{kin} equals an Auger electron energy of an element under investigation: unmonochromatized photons or poor resolution can be employed in order to gain intensity.
- E_{kin} is selected around 2 eV to monitor the secondaries: this yields the highest electron flux with enhanced bulk sensitivity. Contrast is achieved by taking the difference of two images taken at photon energies above and below a core electron threshold energy.

E_{kin} fixed, sweeping $h\nu$: element mapping, CFS

- Photoemission (XPS, UPS) spectra are taken by scanning $h\nu$ for fixed E_{kin}.
- E_{kin} is chosen as discussed for the PEEM mode. When the photon energy sweeps over one of the photoionization thresholds of an element, areas containing this element will show up in the 2D image.
- E_{kin} is set to an Auger transition or to approximately 2 eV using secondary electrons: absorption spectra like EXAFS, NEXAFS or SEXAFS can be recorded from areas down to 1 nm^2. The energy resolution depends, as in the conventional case, just on the monochromator resolution.

4.1.3. *E_{kin} changes: ESCA, AES, CIS*

The kinetic energy is selected with the objective lens acceleration voltage. In this mode the aberration corrector needs to be refocused and readjusted when

E_{kin} is changed. This complicated procedure will be performed completely computer-controlled.

- 20 eV< $h\nu$ < 2000 eV: ESCA and AES analysis with 0.1 eV electron energy resolution.
- With a computer-controlled instrument it is also straightforward to record images in the CIS mode with $h\nu - E_{kin}$ = const.

4.1.4. *Parallel recording of a spectrum from a small area*

The field aperture can be adjusted to select a very small part (down to 5 nm in diameter) of the image in the second entrance plane. The exit slit of the Ω filter is removed and the projective lenses are excited to image the dispersion plane onto the 2D detector. Rapidly changing spectra can thus be acquired with a high dynamic signal range in a bandwidth of about 35 eV.

4.1.5. *Photoelectron diffraction (PED)*

As has already been demonstrated for the SPELEEM,[3] photoelectron diffraction experiments can be easily performed. Compared to the SPELEEM, SMART allows larger acceptance angles for the photoemitted electrons and thus improves the spectral information slightly by monitoring larger emission angles.

4.2. *Imaging rough sample surfaces*

One of the difficulties in PEEM and LEEM is the image distortion when one is investigating rough surfaces due to the relatively high electric field strength. In SMART the front pole piece of the electrostatic–magnetic objective lens can be set to sample potential. Thus the spectromicroscope can be operated with vanishing electric field strength on the sample surface to allow for distortion-free imaging of rough surfaces and with few restrictions for insulator surfaces. However, in this mode E_{kin} should be larger than 500 eV to maintain lateral resolution.

4.3. *Microscopy with an incident electron beam*

Electrons are provided by the electron gun mounted to the beam splitter. For symmetry reasons the illumination energy and the detected energy have to be the same.

4.3.1 *Real image on the detector: LEEM, MEM*

- Incident electrons reach the sample and are scattered by the sample. The scattered electrons are imaged. The achievable lateral resolution should approach the theoretical limit of 0.5 nm in this mode (LEEM).
- Very low energy electrons are reflected by the equipotential surface in front of the sample. MEM is very sensitive to topography and electrical or magnetic microfields on the surface.

4.3.2. *Diffraction plane on the detector: small-spot LEED*

The transfer optics projects the source image into the second entrance plane of the omega filter. Only elastically scattered electrons pass the filter to form the LEED pattern on the detector. With apertures in the electron gun system, the size of the illuminated spot on the sample may be as small as 1μm and therefore on the same length scale as in conventional LEEM's.

5. Using SMART

5.1. *Interactions with the sample*

As in all physical experiments, the sample will be influenced by the measurement itself. Bauer *et al.* have already estimated the advantage of using photoexcitation of image-forming (photo- or Auger) electrons mainly from the significantly improved signal-to-background intensity.[2] Moreover, electron bombardment to stimulate Auger electron emission may lead to severe sample damage (e.g. electron stimulated desorption and dissociation, polymerization of organic adsorbates, etc.) Near-threshold excitation by tunable photon energy using X-ray absorption contrast increases secondary emission, which may furthermore improve the image contrast and reduce possible damage. However, undesired effects like sample heating and photostimulated desorption/dissociation and/or reaction due to the high photon flux have to be taken into account, particularly in conventional adsorbate studies. Desorption due to field emission is negligible in the "rough sample mode," where almost vanishing electric fields act on the sample. In the case of weak physisorptive bonding the influence of the high electric field strength in conventional operation modes can of course not be disregarded.

Heat load

Simple estimations of the heat load on the basis of the prospective photon flux at the PM6 beamline lead to the conclusion that this effect can be mostly disregarded as a limiting factor. In the stationary state upon permanent illumination, heat dissipation into the bulk at the illuminated spot can be described by the Poisson equation, with $K \cdot \nabla\nabla T = -A(r)$, with K being the heat conductivity, T the temperature and A the heat source density.

A very handy solution can be found by approximating the sample by an infinite half space. The heat is uniformly deposited into a circle with radius a. In the center, the increase of temperature will be largest:

$$\Delta T_{\text{disk,center}} = \frac{(1-R)\cdot P \cdot h\nu}{\pi \cdot K \cdot a}.$$

For silicon [K(Si) = 80 Wm^{-1} K^{-1} and negligible reflection coefficient R, total photon flux P of the PM6 beamline = $8.4 \cdot 10^{12}$ photons/s^{-1}, circle radius $a = 4$ μm] the temperature rise ΔT in the center of the disk will be as small as 0.7 K. Estimates for metal substrates are on the same order. A more detailed calculation (not presented here) including the photon absorption properties of the sample reproduces these results within a few percent. Heating is thus negligible for many adsorbate systems.

5.3. *Photodesorption vs. image acquisition time*

Another effect that will be discussed briefly is the influence of photodesorption as a consequence of the photoexcitation/photoionization process. If τ_D is the time it takes to reduce the adsorbed particle density to $1/e$ of its initial value, the number of counts that add up in the detector[16] from one pixel during this time is (for the definition of angles α and β see Fig. 4)

$$\text{counts}(\tau_D) = \rho \cdot P \cdot \frac{\sigma_{\text{Auger}}}{\sigma_D} \; (2\alpha)^2 \cdot \frac{3 \cdot \sin^2\beta}{4 \cdot \pi}$$

Assuming a pixel area P (corresponding to 10 × 10 nm^2 on the sample) and an effective Auger cross section σ_{Auger}, which is about 1000 times larger than the photodesorption cross section σ_D and a particle density ρ of 10^{15} cm^{-2}, the number of counts (τ_D) amounts to 27.000. This means that the number of collected counts before the sample changes is dominated by the ratio of the pixel area and the acceptance angle, and not by the photon flux. The ratio of the two cross sections σ_{Auger} and σ_D depends on the sample for a given photon energy. This means that the pixels can only be made smaller if wide apertures are used or, more important, less sensitive samples are investigated.

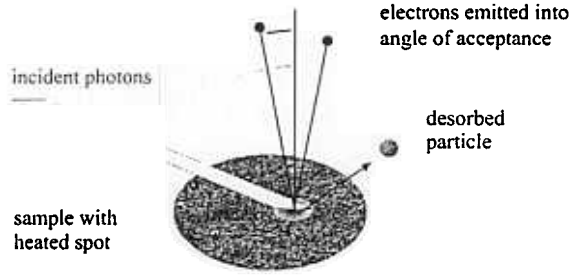

Fig. 4. Interactions of the sample with incident photons: definition of the angles α and β used in the discussion.

6. Conclusions

Aberration correction of a low energy electron microscope in combination with high brilliance synchrotron radiation and a high performance imaging energy filter allows spectroscopic imaging on a length scale of several atomic distances. Whereas in the LEEM mode structural properties of surfaces can be investigated, the versatility of the SMART spectromicroscope, which is planned to start operation at BESSY-II in the year 2000, will enable the most common surface spectroscopy techniques (photoemission and X-ray absorption) on a microscopic scale well beyond the capabilities of existing instruments. Samples may be investigated with only minor influence of electric fields and by photon-induced heating. Aberration correction allows for (and is necessarily required for) both nanometer resolution and significantly enlarged acceptance angles.

Acknowledgments

This project is financed by the Federal German Ministry of Education, Science, Research and Technology (BMBF) under contracts No. 05 644 WWA 9 and No. 05 SL8 WW1 8. R. F. acknowledges financial support by the "Freunde und Förderer der BESSY GmbH" and from the "Jubiläumsstiftung der Universität Würzburg."

References

1. E. Bauer, *Ultramicroscopy* **36**, 52 (1991); L. H. Veneklasen, *Ultramicroscopy* **36**, 72 (1991).
2. E. Bauer, C. Koziol, G. Lilienkamp and T. Schmidt, *J. Electr. Spectrosc. Rel. Phenom.* **84**, 201 (1997).
3. Th. Schmidt, S. Heun, J. Slezak, J. Diaz, K. C. Prince, G. Lilienkamp and E. Bauer, *Surf. Rev. Lett.*, this issue.
4. G. F. Rempfer, D. M. Desloge, W. P. Skozcylas and O. H. Griffith, *Microsc. Microanal.* **3**, 14 (1997)
5. R. Fink, M. R. Weiss, E. Umbach, D. Preikszas, H. Rose, R. Spehr, P. Hartel, W. Engel, R. Degenhardt, H. Kuhlenbeck, R. Wichtendahl, W. Erlebach, K. Ihmann, R. Schlgl, H.-J. Freund, A. M. Bradshaw, G. Lilienkamp, Th. Schmidt, E. Bauer and G. Benner, *J. Electr. Spectrosc. Relat. Phenom.* **84**, 231 (1997).
6. H. Rose, *Optik* **84**, 91 (1989); **85**, 19 (1990).
7. J. Zach, *Optik* **83**, 30 (1989).
8. H. Rose and D. Preikszas, *Optik* **92**, 31 (1992).
9. O. Scherzer, *Optik* **2**, 114 (1947).
10. D. Preikszas and H. Rose, *J. Electr. Micr.* **1**, 1 (1997).
11. H. Rose, D. Krahl, in *Energy-Filtering Transmission Electron Microscopy* (Springer, Berlin, 1995), ed. L. Reimer, p. 43.
12. L. H. Veneklasen, *Rev. Sci. Instrum.* **63**, 5513 (1992).
13. E. Bauer, T. Franz, C. Koziol, G. Lilienkamp and T. Schmidt, in *Chemical, Structural and Electronic Analysis of Heterogenous Surfaces on the Nanometer Scale* (Kluwer, Dordrecht, 1997), ed. R. Rosei, p. 73.
14. Chr. Jung, J. Bahrdt, U. Flechsig and M. R. Weiβ, proc. SPIE (San Diego, 1997), in print.
15. H. Petersen, C. Jung, C. Hellwig, W. B. Peatman and W. Gudat, *Rev. Sci. Instrum.* **66**, 1 (1995)
16. J. Stöhr, *NEXAFS Spectroscopy* (Springer, Berlin, 1992), p. 129.